Rapid and highly selective colorimetric detection of nitrite based on the catalytic-enhanced reaction of mimetic Au nanoparticle-CeO2 nanoparticle-graphene oxide hybrid nanozyme

Adegoke, Oluwasesan; Zolotovskaya, Svetlana A.; Abdolvand, Amin; Nic Daeid, Niamh

Published in:
Talanta

DOI:
10.1016/j.talanta.2020.121875

Publication date:
2021

Rapid and highly selective colorimetric detection of nitrite based on the catalytic-enhanced reaction of mimetic Au nanoparticle-CeO_2 nanoparticle-graphene oxide hybrid nanozyme

Oluwasesan Adegoke[a]*, Svetlana Zolotovskaya[b], Amin Abdolvand[b], Niamh Nic Daeid[a]

[a]*Leverhulme Research Centre for Forensic Science, School of Science & Engineering, University of Dundee, Dundee, DD1 4GH, UK*

[b]*Materials Science & Engineering Research Cluster, School of Science & Engineering, University of Dundee, UK*

* Correspondence: o.adegoke@dundee.ac.uk (OA).

[a] Leverhulme Research Centre for Forensic Science, School of Science & Engineering, University of Dundee, Dundee, DD1 4GH, UK

Abstract

The International Agency for Research cancer (IARC) has classified nitrite in Group 2A of probable carcinogens to human. Herein, we report on the rapid and selective colorimetric detection of nitrite using a chemically modified gold nanoparticle (AuNP)-cerium oxide (CeO_2) NP-anchored graphene oxide (GO) hybrid nanozyme in a catalytic colorimetric assay where nitrite acts as the main oxidant/target analyte and 3,3',5,5'-tetramethylbenzidine (TMB) as the substrate. CeO_2 NPs and GO were synthesized separately and incorporated in-situ, in a synthetic solution involving the chemical reduction of Au salt to AuNPs. The chemical modification process aided the adsorption of CeO_2 NPs and AuNPs on GO nanosheets, yielding a highly catalytic AuNP-CeO_2 NP@GO nanohybrid material. Under optimum experimental conditions, a novel colorimetric assay for nitrite recognition was constructed in which AuNP-CeO_2 NP@GO hybrid nanozyme catalysed the oxidation of TMB in the presence of nitrite prepared in a 2-(n-morpholino)ethanesulfonic acid-2-[bis(2-hydroxyethyl)amino]-2-(hydroxymethyl)propane-1,3-diol-tris(hydroxymethyl)aminomethane acetate (MES-BIS-TRIS-Trisma Ac)-citric acid buffer solution, pH 2. Nitrite was quantitatively detected in a concentration dependent manner from 100 μM to 5000 μM with a correlation coefficient of 0.9961 and a limit of detection of 4.6 μM. Selective detection of nitrite was confirmed by the generation of a unique green colour reaction upon nitrite interaction in the AuNP-CeO_2 NP@GO hybrid nanozyme redox cycle with TMB. None of the several tested metal ions and including H_2O_2 yielded a positive colour response, thus demonstrating the superior selectivity of the catalytic colorimetric assay for nitrite recognition. The AuNP-CeO_2 NP@GO hybrid nanozyme catalytic colorimetric assay was successfully applied in the detection of nitrite in tap water.

KEYWORDS: Colorimetric; nanohybrid; nanozyme; oxidation; nanoparticle

1. Introduction

Artificial enzyme, a terminology coined by Ronald Breslow is a promising and expansive field of biomimetic chemistry which uses alternative types of materials to mimic the general and essential properties of natural enzymes **[1,2].** Amongst the various artificial enzymes developed to date, nanomaterials-based enzyme mimics, known as nanozymes have been widely used in several fields of research such as pollutant removal, stem cell growth, neuroprotection, cancer therapy and in sensor/biosensor applications **[3]**. Since the peroxidase mimetic activity of iron oxide nanoparticles (NPs) was reported in 2007 **[4]**, several other metal oxide nanomaterials such as cerium oxide (CeO_2) NPs also known as nanoceria **[5]**, cobalt oxide **[6]**, metal-based nanomaterials (e.g. gold (Au) NPs and platinum NPs) **[7,8]** and carbon-based nanomaterials **[9]** have been reported as nanozymes and used in the development of oxidase, catalase or peroxidase-mimic sensor systems. Since the efficiency of catalytic signals varies amongst nanomaterials, the formation of hybrid nanozymes have been used as a strategy to enhance catalytic signals in oxidase or peroxidase mimic assays **[10,11].** Hence, there is a continuous interest in the development of nanozyme-based catalytic colorimetric sensors for the detection of a wide range of chemical and biological analytes.

The ubiquitous prevalence of nitrite in the environment occurs due to the pervasive use of nitrogen-rich nutrients. For example, nitrite association with underground water and natural surfaces is necessitated by the important role it plays in biogeochemical nitrogen cycle **[12]**. Nitrification-denitrification reaction process of wastewater contains rich ammonium ion that releases nitrite as oxidative products into waterways **[13].** In the food industry, the preservation of meat from spoilage using nitrite salts (sodium nitrite and potassium nitrite) as curing mixture is a common means for nitrite ingestion **[14].** The International Agency for Research cancer (IARC) has classified nitrite in Group 2A of probable carcinogens to human **[15].** The extended release and consumption of nitrite can cause stomach cancer, hypertension, thermo-globinemia, congenital disabilities and spontaneous abortions **[16]**.

Nitrite also plays a crucial role in the area of forensic science because of its association with some explosive compounds and with gunshot residues that diffuse out from the propellant charge when a firearm is discharged. Nitrite is an important inorganic component of this gunshot residue **[17,18].** The traditional Griess Assay which was developed in 1879 was the most commonly used method

for the spectrophotometric detection of nitrite **[19]**. However, due to the carcinogenic property of the 1-naphthylamine reagent used in the diazo-coupling reaction, modification to the Griess Assay was implemented by Bratton in 1939 **[20]** in which N-(1-naphthyl)ethylenediamine was used instead of the 1-naphthylamine reagent. Since then, the modified Griess Assay has been used as the standard method for nitrite detection. However, false positive results from ions such as Fe^{3+}, I^-, S^{2-} and Cu^{2+} have limited its use **[19].** Due to this limitation, several other methods for nitrite detection have been developed over the years but these methods also have their drawbacks. For example, HPLC-coupling Griess assay systems are complex, expensive and suffer from interference from ions such as Cl^- **[19]**. Catalytic-based spectrophotometric assays suffers from poor biocompatibility and are time consuming **[19]**. Chemiluminescence-based methods are easily affected by poor stability, poor reproducibility and environmental factors **[21]** and electrochemistry techniques suffer from interferences **[19].** Due to these limitations, there is a considerable interest in the development of simple, cost-effective, sensitive, selective and rapid detection systems for nitrite recognition and a promising direction is the use of hybrid nanozymes in catalytic-based assays.

In this work, we report on the chemical modified synthesis of AuNP-CeO_2 NP@graphene oxide (GO) nanohybrid material and its use as an artificial enzyme mimic for the colorimetric detection of nitrite. The novel colorimetric assay developed in this work, showed that the AuNP-CeO_2 NP@GO hybrid nanozyme can rapidly catalyse the oxidation of 3,3',5,5'-tetramethylbenzidine (TMB) in the presence of nitrite to generate a unique green colour. To the best of our knowledge, this is the first reported hybrid nanozyme that functions as a catalyst to oxidize TMB in the presence of nitrite to generate a specific unique green colour. Also, as hydrogen peroxide (H_2O_2) is widely used as the oxidant/recognition analyte in peroxidase mimic assays, our work is the first reported use of nitrite as an oxidant/recognition analyte in a novel colorimetric assay involving the catalytic oxidation of TMB by nitrite.

2. Experimental

2.1. Materials

Silver nitrate ($AgNO_3$), 2-[Bis(2-hydroxyethyl)amino]-2-(hydroxymethyl)propane-1,3-diol (BIS-TRIS), tris(hydroxymethyl)aminomethane acetate (Trizma Ac), H_2O_2 (30% w/w) in solution with stabilizer

and citric acid, cerium (III) nitrate hexahydrate, zinc chloride and sodium acetate (NaAc) were purchased from Sigma Aldrich. Sodium nitrite and sodium sulphate anhydrous were purchased from VWR Chemicals. Iron (III) chloride hexahydrate, sodium nitrate, nickel chloride hydrate and lead chloride were purchased from Acros Organics. Ammonium hydroxide, 2-(n-morpholino)ethanesulfonic acid (MES), TMB, gold (III) chloride trihydrate ($HAuCl_4.3H_2O$) potassium acetate (KAc), potassium permanganate ($KMnO_4$), graphite powder, barium chloride dihydrate, copper chloride dihydrate, tin chloride dihydrate and magnesium chloride hexahydrate were purchased from Thermo Fisher. The buffer solution used in this study was prepared in ultrapure Milli-Q water (H_2O).

2.2. Equipment

Absorption measurements were carried out using an ultraviolet/visible (UV/vis) Cary Eclipse (Varian) spectrophotometer from Agilent. Morphological characterization of the nanomaterials was carried out using transmission electron microscopy (TEM) JEOL JEM-1200EX operated at 80 kV and with scanning electron microscope (SEM) JEOL JSM 7400F field emission from JEOL. Elemental analysis of the hybrid nanomaterials was carried out using energy dispersive X-ray spectroscopy (EDX) integrated with SEM. Dynamic light scattering (DLS) hydrodynamic particle size and zeta potential analysis were carried out using Zetasizer Nano ZS series (ZEN3600 from Malvern Panalytical). Colorimetric absorbance signals were measured from an 800 TS microplate absorbance reader from BioTek. Raman spectra were collected using a set-up built in-house, comprising a microprobe system equipped with a continuous wave laser sources emitting at 633 nm, the Oriel MS257 monochromator fitted with the Andor Newton EMCCD detector TE cooled to -70°C. The backscattering configuration was used for the signal collection. The incident power on the samples was 7 mW. The spectra were recorded using a 40x objective, a 1 s accumulation time with a total of 10 accumulations. Powder X-ray Diffraction (PXRD) analysis was carried out using a Siemens D5000 diffractometer with copper (Cu) Kα radiation (λ=1.54056 nm) whilst data were obtained in the range of 3-60° using a 0.1° 2θ step size and a 3 s count time per step with a 0.066° slit width. FT-IR analysis was carried out using an Agilent Cary 630 FT-IR spectrometer.

2.3. Synthesis of AuNP-CeO_2 NP@GO nanohybrid

GO was synthesized according to a modified method previously reported by our group **[22].** Firstly, graphite oxide was synthesized by mixing 1.25 g sodium nitrate and 2.5 g graphite powder in 60 mL ice-cooled solution of sulphuric acid. Once homogenous dispersion of graphite was achieved, 7.5 g potassium permanganate was added and the solution was stirred for ~24 hours (hr) after being kept under ice for ~2 hr. Thereafter, 75 ml Milli-Q H_2O was slowly added and the reaction mixture was stirred for another ~24 hr at ~100 ºC. After cooling the reaction down, 35% H_2O_2 (25 mL) was added and the formed graphite oxide was purified with 5% hydrochloric acid and acetone via centrifugation and thereafter dried in a fume hood. GO was obtained via exfoliation by ultrasonicating the synthesized graphite oxide, purifying with acetone and thereafter dried.

CeO_2 NPs were synthesized via a modified method **[23]** by mixing 2.5 g cerium (III) nitrate hexahydrate in 90 mL H_2O:ethylene glycol (50:50) and heating to ~60 °C under reflux. Thereafter, 15 mL NH_4OH (28%) was slowly added and the solution was stirred for ~1 hr 30 minutes (min), reaching a temperature of 75 °C. The product was thereafter purified using ethanol via centrifugation and dried. Surface functionalization was carried out by dissolving the CeO_2 NPs in 100 mL aqueous solution containing 0.2 g of trisodium citrate. The solution was stirred for few minutes (min), purified via centrifugation with ethanol and later dried in the fume hood.

To prepare the AuNP-CeO_2 NP@GO nanohybrid (Scheme 1), hydrothermal reduction of Au salt to AuNPs were first carried out. Briefly, under reflux, 1 mL of 1% $HAuCl_4.3H_2O$ solution in 79 mL Milli-Q H_2O was mixed with 20 mL aqueous solution containing 4 mL 1% trisodium citrate, 1 mL 1% $NaBH_4$ and 15 mL Milli-Q H_2O. Once the citrate-AuNPs were formed, 5 mL aqueous solution of GO (15 mg GO in Milli-Q H_2O) and 10 mL aqueous solution of citrate-CeO_2 NPs (0.2 g in in Milli-Q H_2O) were added and the solution was stirred for ~30 min, reaching a temperature of ~80 °C. The AuNP-CeO_2 NP@GO nanohybrid product was purified via filtration and stored at 4 °C prior to use. Our analysis showed that after ~10 months, AuNP-CeO_2 NP@GO was still highly stable as judged by the UV/vis absorption spectrum of the projected surface plasmon resonance (SPR) absorption peak which did not diminish, broadened or shift to the red region (Fig. S1).

2.4. Assay procedure

To selectively detect nitrite, a novel buffer solution was developed for effective catalytic reaction and for pH control of the colorimetric reaction process. Under optimized experimental conditions, 200 µL of the AuNP-CeO_2 NP@GO nanohybrid solution (0.02 nM) was mixed with 90 µL of 0.8 mM TMB (prepared in citrate-phosphate buffer pH 3.0) and 60 µL of appropriate nitrite concentration prepared in MES-BIS TRIS-Trisma Ac-citric acid buffer, pH 2.0. The catalytic assay was left to react for 1 min 30 seconds (sec) after adding the appropriate nitrite concentration and the generated catalytic colorimetric signal was recorded via an 800 TS microplate absorbance reader from BioTek.

3. Results and discussion

3.1. Characterization

3.1.1 SEM, EDX and TEM analysis

Graphene is conceptually flat and characterized by arrays of sp^2 trigonal hybridized carbon atom sheets. Under strong acidic and oxidative reaction, graphite oxide was chemical exfoliated to GO, generating oxygen atoms with embedded functional moieties such as esters, epoxides, hydroxyls and carboxyls that lie on the basal planes and within the carbon-arrayed graphene nanosheets **[24,25]**. The high surface area, arrayed carbon layers and accessible pores, allows GO to be an excellent adsorbent for other materials. Citrate-AuNPs and citrate-CeO_2 NPs were chemically adsorbed on GO nanosheets in-situ, and we have used SEM and TEM to characterize the surface morphology of the resultant AuNP-CeO_2 NP@GO nanohybrid material. Fig 1A and B shows the SEM images of the nanohybrid material taken at different magnifications. From the SEM images, we observed a combination of clumped particles of AuNP-CeO_2 NPs spread across the surface of crumpled flaky sheets of stacked, folded and wrinkled GO. The observed morphological feature provides a strong affirmation that AuNP-CeO_2 NPs were effectively anchored onto GO nanosheets. The adsorption process could be either of hydrogen bonding or van der Waals interactions.

Quantitative and qualitative elemental composition of the AuNP-CeO_2 NP@GO nanohybrid material was analysed using EDX. As shown in Fig. S2, peaks corresponding to the elemental components of the nanohybrid materials, i.e., carbon (present in GO), oxygen (present in GO and CeO_2 NPs), cerium (present in CeO_2 NPs) and Au (present in AuNPs) were vividly projected in the displayed

EDX spectrum. The weight percentage (%) of C (21.47%), O (24.68%), Ce (51.20%) and Au (2.64%) obtained, showed that the nanohybrid material was composed of AuNPs, CeO_2 NPs and GO.

Further surface morphological characterization of the nanohybrid material was carried out using TEM. Fig. 1C and D shows TEM images of the AuNP-CeO_2 NP@GO taken at different positions on the pioloform-coated grid surface. From the images, it is evident that GO was characterised by individual well-exfoliated sheets with the absence of bulk aggregates. AuNP-CeO_2 NPs nanohybrid appeared as clumps of aggregates across the GO nanosheet surface and was indicative of the nanohybrid material adsorption on GO nanosheet.

3.1.2. PXRD analysis

The crystal phase structure of AuNP-CeO_2 NP@GO was characterised using PXRD. As shown in Fig. 2A, the diffraction peak at plane {002} was well projected in the diffraction pattern for GO and moderately projected in the diffraction pattern for AuNPs and CeO_2 NPs. The multi-layered array of GO nanosheets may be indicative of the well pronounced diffraction peak at plane {002}. In the diffraction pattern of AuNP-CeO_2 NP@GO, the diffraction peak at plane {002} was evidently projected while the diffraction peaks at plane {122} and {210} corresponded relatively to the diffraction peaks of citrate-AuNPs and CeO_2 NPs observed in the Bragg angle region of their diffraction pattern.

3.1.3. DLS and Zeta potential

DLS was used to probe the hydrodynamic size of the AuNP-CeO_2 NP@GO nanohybrid material in solution and the value obtained was alternatively used to examine the agglomeration state of the material. A hydrodynamic size value greater than 100 nm is indicative of the colloidal state of the nanohybrid material being polydisperse while a size value less than 100 nm is indicative of a monodisperse colloidal state. Fig. 2B shows the DLS histogram plot of the AuNP-CeO_2 NP@GO nanohybrid material in which the hydrodynamic size value obtained was 96.8 nm. The obtained value tentatively proved the monodisperse colloidal state of the nanohybrid material.

Zeta potential was used to probe the surface charge and colloidal stability of the nanohybrid material. Generally, zeta potential value of ±30 mV corresponds to a highly stable NP dispersion, ±20-30 mV as moderately stable, ±10-20 mV as relatively stable and ±0-10 mV as highly unstable. Fig. 2C shows the zeta potential plot of the AuNP-CeO_2 NP@GO nanohybrid material. From the plot, the measured zeta potential value was -36.3 mV which showed that the nanohybrid material was highly stable.

3.1.4. Raman analysis

Raman analysis of the AuNP-CeO_2 NP@GO nanohybrid material was carried out to further understand the materials structural properties. As shown in Fig. 3A, the Raman spectrum of GO was characterised by two prominent peaks at 1325 cm^{-1} and 1557 cm^{-1} which corresponds to the characteristic D and G bands. The D band is attributed to the size decrease of the sp^2 domain caused by the strong oxidising state of the graphene nanosheets. The G band on the other hand arises due to the first order E_{2g} scattering **[26].** Evaluating the Raman spectrum of AuNP-CeO_2 NP@GO relative to GO, we observed a shift to higher wavenumber in the D (1341 cm^{-1}) and G (1600 cm^{-1}) bands and the emergence of a new peak at 447 cm^{-1}. Prior to the adsorption of AuNPs and CeO_2 NPs on GO, the intensity ratio I_D/I_G for GO was 1.13 but increased to 1.27 for the AuNP-CeO_2 NP@GO nanohybrid. The increase suggest that the graphitic domain of GO was influenced by the adsorptive effects of AuNPs and CeO_2 NPs.

3.1.5. FTIR analysis

FTIR analysis was carried out to characterize the functional groups on AuNP-CeO_2 NP@GO and the individual material component of the nanohybrid. Fig. 3B shows the FTIR spectra of citrate-AuNPs, citrate-CeO_2 NPs, GO and AuNP-CeO_2 NP@GO. For citrate-AuNPs, the peaks at 1558 cm^{-1} can be attributed to the asymmetric COO- stretching band while the three peaks at 1392 cm^{-1}, 1361 cm^{-1} and 1352 cm^{-1} can be attributed to the symmetric COO- stretching band. For CeO_2 NPs, the peaks at 1634 cm^{-1}, 1439 cm^{-1}, 1064 cm^{-1} and 1520 cm^{-1} can be assigned to the N-H stretching, C-H bend, C-O stretching and Ce-O stretching bands respectively. For GO, the peaks at 1704 cm^{-1}, 1258 cm^{-1}

and 1030 cm^{-1} can be assigned to the carbonyl (C=O), epoxy (C-O) and alkoxy (C-O) functional groups. For AuNP-CeO_2 NP@GO, the peak at 1560 cm^{-1} can be assigned to the asymmetric COO- stretching band present in citrate-AuNPs while the peak at 1093 cm^{-1} can be assigned to the alkoxy (C-O) functional groups present in GO and the peak at 469 cm^{-1} can be assigned to the Ce-O stretching band found in citrate-CeO_2 NPs.

3.2. Catalytic activity

The catalytic activity of the AuNP-CeO_2 NP@GO hybrid nanozyme towards nitrite recognition was investigated. As shown in Fig. 3Ci, the UV/vis spectrum of the AuNP-CeO_2 NP@GO nanohybrid featured a characteristic SPR absorption peak around 520 nm. Reaction of the hybrid nanozyme with nitrite (Fig. 3Cii), MES-BIS-TRIS Trisma Ac-citric acid buffer, pH 2 (Fig. 3Ciii), and TMB (Fig. 3Civ), induced the SPR absorption peak to weaken and broaden with no catalytic absorption peak formation. When the hybrid nanozyme was mixed with TMB and the MES-BIS-TRIS Trisma Ac-citric acid buffer (without nitrite), the SPR absorption peak still weakened with no apparent catalytic absorption formation (Fig. 3Cv). However, when the hybrid nanozyme was mixed with TMB and MES-BIS-TRIS Trisma Ac-citric acid buffered nitrite solution, a well projected catalytic absorption peak with a wavelength maximum around 650 nm and a strong greenish colorimetric reaction was observed (Fig. 3Cvi). This proves to show that AuNP-CeO_2 NP@GO hybrid nanozyme functioned as an artificial enzyme mimic for the colorimetric recognition of nitrite.

3.3. Assay optimization

3.3.1. Effects of buffer and pH

The effects of buffer and pH on the catalytic activity of the AuNP-CeO_2 NP@GO hybrid nanozyme towards nitrite recognition was studied in comparison to other nanozymes and nanomaterials. The term “Good buffers” was used to represent buffers with catalytic stabilizing properties in enzymatic assays **[27].** Discovering the appropriate buffer system needed for optimum catalytic reaction is very challenging due to the varying interactions of each analyte to a particular buffer system. In this work, five different buffer systems were prepared and the catalytic activities of AuNP-CeO_2 NP@GO, AgNP-CeO_2 NP@GO, AuNP@GO, CeO_2 NP, citrate-AuNPs and GO towards nitrite recognition was

investigated. As shown in Fig. 4A, the catalytic signal of AuNP-CeO_2 NP@GO for nitrite recognition in MES-BIS-TRIS-Trisma Ac-citric acid and BIS-TRIS-Trisma Ac-KAc-NaAc-citric acid buffer was more enhanced than the rest of the nanomaterials tested and the other tested buffer system. We found the catalytic signal of AgNP-CeO_2 NP@GO to be the weakest within the optimized experimental conditions used for nitrite detection. The result clearly shows that the nature of the buffer system used in the colorimetric assay played an important role in the induced catalytic signal. Hence, we chose MES-BIS-TRIS-TrismaAc-citric acid as the choice buffer system for nitrite recognition.

Fig. 4B and 4C shows the photographic colorimetric response and the corresponding catalytic signal of AuNP-CeO_2 NP@GO, AgNP-CeO_2 NP@GO, AuNP@GO, CeO_2 NP, citrate-AuNPs and GO at different pH for nitrite recognition in BIS-TRIS-TrismaAc-citric acid buffer system. From the displayed photographic colorimetric response, AuNP-CeO_2 NP@GO induced a strong green colour reaction at pH 2.0, which thereafter weakened as the pH of the solution increased. For the rest of the nanomaterials tested, CeO_2 NPs, AuNP@GO and GO displayed moderate colour reactions across the pH range studied with the colour reaction mostly weakened at higher pH. Judging from the corresponding catalytic signal of the tested nanomaterials, superior catalytic response for nitrite recognition was observed for AuNP-CeO_2 NP@GO hybrid nanozyme at pH 2. The observed results tentatively confirm AuNP-CeO_2 NP@GO as a superior nanohybrid artificial enzyme for nitrite colorimetric detection and pH 2 was selected as the choice pH for the catalytic reaction.

3.3.2. Effect of assay time

The effect of assay time was probed to effectively optimize the catalytic colorimetric reaction for nitrite recognition. As shown in Fig. 5A, the photographic colorimetric response of AuNP-CeO_2 NP@GO hybrid nanozyme triggered a green catalytic colour reaction within 30 sec for nitrite. With prolonged time period, the green colour reaction was stronger and thereafter began to fade steadily and eventually turned brown. The corresponding time-dependent AuNP-CeO_2 NP@GO catalytic signal for nitrite recognition (Fig. 5B) showed that the catalytic rate of reaction occurred rapidly within 30 sec, reached optimum signal at 1 min 30 sec and decreased steadily with time. Based on the observed results, we chose 1 min 30 sec as the optimum assay time for nitrite colorimetric detection.

3.3.3. Effect of TMB

The AuNP-CeO_2 NP@GO catalytic signal response to nitrite recognition in the presence of varying concentrations of TMB substrate (0.8 mM to 3.0 mM) and a fixed concentration of nitrite (5000 μM) was investigated. As shown in Fig. S3, the catalytic absorbance signal increased steadily from 0.8 mM and reached optimum signal at 1.2 mM TMB concentration. Thereafter, the catalytic absorbance signal began to decrease in direct relationship to increasing concentration of TMB. Based on the observed result, we chose 1.2 mM as the choice TMB concentration for nitrite recognition.

3.4. Reaction mechanism

Scheme 1 provides a descriptive illustration of the catalytic reaction mechanism for nitrite detection. In the presence of nitrite, AuNP-CeO_2 NP@GO hybrid nanozyme catalysed the oxidation of TMB to generate a green coloured product specific to nitrite. Generally, the initiation of a catalyst enzyme-induced colour reaction for signal reporting is dependent upon the presence of an oxidizing agent to initiate the redox reaction. H_2O_2 has been the most popular oxidant used in nanozyme redox cycle reaction of which several sensors and biosensors have been developed **[28,29]**. In our work, the catalytic colorimetric assay was designed to selectively recognise nitrite as the oxidant in the hybrid nanozyme redox cycle initiation. The ability of nitrite to act as an oxidizing agent is predominantly attributed to the N-O covalent linkage low bond energy which has been reported to be 53 kcal/mol **[30]**. The low N-O energy bond feature allows nitrite to act as a potent electrophilic oxidant as evidenced by its relatively high redox potential **[31].** Since AuNP-CeO_2 NP@GO behaves as an artificial enzyme mimic, nitrite is expected to be able to migrate to the materials interface where it binds and react with the redox site of the hybrid nanozyme. A more logical approach in describing the chemical interactive relationship between AuNP-CeO_2 NP@GO, nitrite and TMB would be according to the redox cycle initiation in which nitrite analyte acts as the oxidizing agent and the completion of the redox cycle reaction where TMB acts as the electron donating reducing agent. A proposed catalytic redox reaction pathway for nitrite incorporating both oxidation and reduction reactions within our hybrid nanozyme redox cycle can be described sequentially by four chemical reaction equations:

$AuNP\text{-}CeO_2$ NP@GO + NO_2^- + → [$AuNP\text{-}CeO_2$ NP@GO]* + NO (1)

[$AuNP\text{-}CeO_2$ NP@GO]* + XH_2 → [$AuNP\text{-}CeO_2$ NP@GO]** + XH• (2)

[$AuNP\text{-}CeO_2$ NP@GO]** + XH_2 → $AuNP\text{-}CeO_2$ NP@GO + XH• (3)

$2XH_2 + NO_2^- \rightarrow NO + H_2O + 2XH•$ (4)

XH_2 in the $AuNP\text{-}CeO_2$ NP@GO redox cycle is used to denote the TMB substrate. According to the proposed equation, activation of the $AuNP\text{-}CeO_2$ NP@GO redox cycle is triggered through the electron oxidation of $AuNP\text{-}CeO_2$ NP@GO event which is initiated by the oxidized nitrite. Occurring as an electron oxidation of the $AuNP\text{-}CeO_2$ NP@GO active site, the native $AuNP\text{-}CeO_2$ NP@GO is converted to a highly oxidative state specie denoted as [$AuNP\text{-}CeO_2$ NP@GO]* **[32].** The electron oxidation reaction induced by nitrite then led to the formation of [$AuNP\text{-}CeO_2$ NP@GO]**, which describes the intermediate oxidation state. Therefore, it is imperative to say that [$AuNP\text{-}CeO_2$ NP@GO]* oxidising power is the main driving force that converts colourless TMB to the green coloured oxidised product used for the selective signal recognition of nitrite. A simplified description of the $AuNP\text{-}CeO_2$ NP@GO redox cycle is shown in Scheme 1.

3.5. Selectivity

The efficacy of $AuNP\text{-}CeO_2$ NP@GO hybrid nanozyme to function as a highly selective catalytic colorimetric sensor for nitrite was investigated. Different metal ions having the tendency to act as interferents were subjected to the same catalytic assay condition as nitrite and the generated responses were recorded. As shown in Fig 6A, none of the tested metal ions and H_2O_2 triggered a positive colorimetric response in a similar fashion to the deep green colour reaction observed for nitrite. Fig 6B shows the corresponding catalytic absorbance signal of nitrite in comparison to the response generated from the tested metal ions and H_2O_2. From the observed data, it is evident that the $AuNP\text{-}CeO_2$ NP@GO hybrid nanozyme is strongly selective to nitrite based on the superior catalytic signal generated in comparison to the non-catalytic response from the tested metal ions and H_2O_2. Therefore, we can tentatively affirm that $AuNP\text{-}CeO_2$ NP@GO hybrid nanozyme functions selectively as a catalytic colorimetric sensor for nitrite without H_2O_2 present in the assay system.

3.6. Quantitative detection

Quantitative detection of nitrite is important so as to determine the amount of nitrite in a given sample. Knowing the amount of nitrite can help in assessing the toxicity level and ensuring the value is below or within the acceptable limit of detection. As a result, several methods have reported on nitrite detection, based on kinetic studies and quantitative analysis **[33-38]**.

In this work, quantitative detection of nitrite under optimum experimental conditions using the AuNP-CeO_2 NP@GO hybrid nanozyme was carried out. The photographic colorimetric response in the concentration range of (100 – 5000 μM) is shown in Fig. 7A. At low concentration of nitrite, a faint green colour reaction was visible and as the concentration of nitrite increased in the assay system, the green colour reaction steadily turned deeper green. The UV/vis absorption spectra shown in Fig. S4, reveals a steady increase in the catalytic absorption signal as the concentration of nitrite increased in the assay system. The plot of the generated quantitative catalytic signal against the detected nitrite concentration shown in Fig. 7B, revealed a linear regression plot with a correlation coefficient of 0.9961. From the linear regression plot, we determined the limit of detection (LOD) and limit of quantitation (LOQ) by multiplying the standard deviation of blank measurements (n = 10) by 3 (LOD) and 10 (LOQ) and dividing by the slope of the graph. The calculated LOD for nitrite was 4.6 μM (0.3 μg/mL) and is 10-fold lower than the limit of 3 mg/L set by the World Health Organization **[39].** The calculated LOQ was ~1.0 μg/mL. The analytical parameters of the AuNP-CeO_2 NP@GO hybrid nanozyme for nitrite detection are summarised in Table 1 and are compared with published colorimetric analytical data for nitrite. Based on the comparison, it is evident that the sensitivity and response time of the AuNP-CeO_2 NP@GO hybrid nanozyme towards nitrite recognition is more superior to the published analytical parameters.

3.7. Detection in tap water

Application of the AuNP-CeO_2 NP@GO catalytic colorimetric assay to detect nitrite in tap water was carried out. Tap water obtained from our lab was spiked with nitrite concentrations of 5000 μM, 3000 μM, 1000 μM and 500 μM. As shown in Table 2, the recovery rate of nitrite in tap water in all tested concentration was greater than 60% with 500 μM nitrite concentration giving a recovery rate as high

as 87%. The relative standard deviation (RSD) was between (0.4-1.7%) demonstrating the excellent reproducibility of the catalytic colorimetric sensor toward nitrite detection in tap water.

4. Conclusions

GO nanosheet and citrate-CeO_2 NPs were synthesized and incorporated in-situ in a synthetic solution where Au salt was chemical reduced to AuNPs. The preparation process aided the direct adsorption of AuNPs and CeO_2 NPs on GO nanosheet leading to the formation of a highly catalytic AuNP-CeO_2 NP@GO nanohybrid material. The nanohybrid material was characterized using a combination of electron microscopy, X-ray diffraction and spectroscopic techniques. A novel colorimetric assay for nitrite was thereafter developed in which AuNP-CeO_2 NP@GO nanohybrid acted as an artificial enzyme mimic to catalyse the oxidation of TMB in the presence of nitrite. The ability of nitrite to act as a suitable oxidant within the AuNP-CeO_2 NP@GO-TMB redox cycle and generate a unique green colour reaction, formed the basis for the selective catalytic colorimetric detection of nitrite. None of the tested metal ions and including H_2O_2 triggered a positive catalytic response to the AuNP-CeO_2 NP@GO colorimetric probe, thus demonstrating the unique selectivity of the nitrite colorimetric sensor. Under optimum experimental conditions, nitrite was quantitively detected within the concentration range of 100 – 5000 µM with a LOD of 0.3 µg/mL. The colorimetric probe was successfully applied for nitrite detection in tap water.

Acknowledgements

Authors gratefully acknowledge the support from Leverhulme Trust for funding this work. SZ acknowledges support from EPSRC through EP/P008135/2 and EP/S017445/1.

Appendix A. Supporting information

Supplementary data associated with this article can be found in the online version at doi:

References

[1] R. Breslow, L.E. Overman, "Artificial enzyme" combining a metal catalytic group and a hydrophobic binding cavity, J. Am. Chem. Soc. 92 (1970) 1075–1077, https://doi.org/10.1021/ja00707a062.

[2] A.J. Kirby, F. Hollfelder, From enzyme models to model enzymes, Royal Society of Chemistry, Cambridge, 2009.

[3] H. Wei, E. Wang, Nanomaterials with enzyme-like characteristics (nanozymes): next-generation artificial enzymes, Chem. Soc. Rev. 48 (2019) 1004-1076, https://doi.org/10.1039/C8CS00457A.

[4] L.Z. Gao, J. Zhuang, L. Nie, J.B. Zhang, Y. Zhang, N. Gu, T.H. Wang, J. Feng, D.L. Yang, S. Perrett, X. Yan, Intrinsic peroxidase-like activity of ferromagnetic nanoparticles, Nat. Nanotechnol. 2 (2007) 577-583, doi: 10.1038/nnano.2007.260.

[5] I. Celardo, J. Z. Pedersen, E. Traversa and L. Ghibelli, Pharmacological potential of cerium oxide nanoparticles, Nanoscale 3 (2011) 1411–1420, https://doi.org/10.1039/C0NR00875C.

[6] J. F. Yin, H. Q. Cao and Y. X. Lu, Self-assembly into magnetic Co_3O_4 complex nanostructures as peroxidase, J. Mater. Chem. 22 (2012) 527–534, https://doi.org/10.1039/C1JM14253D.

[7] X. X. Zheng, Q. Liu, C. Jing, Y. Li, D. Li, W. J. Luo, Y. Q. Wen, Y. He, Q. Huang, Y. T. Long and C. H. Fan, Angew. Chem. Catalytic gold nanoparticles for nanoplasmonic detection of DNA hybridization, Int. Ed. 50 (2011) 11994–11998, https://doi.org/10.1002/anie.201105121.

[8] L. B. Zhang, L. Laug, W. Munchgesang, E. Pippel, U. Gosele, M. Brandsch and M. Knez, Reducing Stress on Cells with Apoferritin-Encapsulated Platinum Nanoparticles, Nano Lett. 10 (2010) 219–223, https://doi.org/10.1021/nl903313r.

[9] R. J. Cui, Z. D. Han and J. J. Zhu, Helical carbon nanotubes: intrinsic peroxidase catalytic activity and its application for biocatalysis and biosensing, Chem.–Eur. J. 17 (2011) 9377–9384, https://doi.org/10.1002/chem.201100478.

[10] G.H. Jin, E. Ko, M.K. Kim, V.-K. Tran, S.E. Son, Y. Geng, W. Hur, G.H. Seong, Graphene oxide-gold nanozyme for highly sensitive electrochemical detection of hydrogen peroxide, Sens. Actuators B Chem. 274 (2018) 201-209, https://doi.org/10.1016/j.snb.2018.07.160.

[11] O. Adegoke, S. Zolotovskaya, A. Abdolvand, N. Nic Daeid, Biomimetic graphene oxide-cationic multi-shaped gold nanoparticle-hemin hybrid nanozyme: Tuning enhanced catalytic activity for the rapid colorimetric apta-biosensing of amphetamine-type stimulants, Talanta 216 (2020) 120990, https://doi.org/10.1016/j.talanta.2020.120990.

[12] I. Wolff, A. Wasserman, Nitrates, nitrites, and nitrosamines, Science 177 (1972) 15–19, DOI: 10.1126/science.177.4043.15.

[13] Y. Miao, L. Zhang, B. Li, Q. Zhang, S. Wang, Y. Peng, Enhancing ammonium oxidizing bacteria activity was key to single-stage partial nitrification-anammox system treating low-strength sewage under intermittent aeration condition, Bioresour. Technol. 231 (2017) 36–44, https://doi.org/10.1016/j.biortech.2017.01.045.

[14] L. Leistner, Hurdle Technology Applied to Meat Products of the Shelf Stable Product and Intermediate Moisture Food Types, Properties of Water in Foods, Springer, 1985, pp. 309–329.

[15] K. Vellingiri, V. Choudhary, L. Philip, Fabrication of portable colorimetric sensor based on basic fuchsin for selective sensing of nitrite ions, J. Environ. Chem. Eng. 7 (2019) 103374, https://doi.org/10.1016/j.jece.2019.103374.

[16] Y. Xiong, C.-J. Wang, T. Tao, M. Duan, S.-W. Fang, M. Zheng, A miniaturized fibreoptic colorimetric sensor for nitrite determination by coupling with a microfluidic capillary waveguide, Anal. Bioanal. Chem. 408 (2016) 3413–3423, https://doi.org/10.1007/s00216-016-9415-1.

[17] N. Petraco, M. Yander, J. Sardone, Method for the quantitative determination of nitrites in gunshot residue cases, Forensic Sci. Int 18 (1981) 85-92, https://doi.org/10.1016/0379-0738(81)90143-2.

[18] F. Tagliaro, F. Bortolotti, G. Manetto, V.L. Pascali, M. Marigo, Dermal nitrate: an old marker of firearm discharge revisited with capillary electrophoresis, Electrophoresis 23 (2002) 278-282, https://doi.org/10.1002/1522-2683(200202)23:2<278::AID-ELPS278>3.0.CO;2-Q.

[19] Q.-H. Wang, L.-J. Yu, Y. Liu, L. Lin, R.-G. Lu, J.-P. Zhu, L. He, Z.-L. Lu, Methods for the detection and determination of nitrite and nitrate: A review, Talanta 165 (2017) 709-720, https://doi.org/10.1016/j.talanta.2016.12.044.

[20] E.K.M.A. Calvin Bratton Jr. With the technical assistance of Dorothea Babbitt and Alma R. Hendrickson, A new coupling component for sulfanil-amide determination, J. Biol. Chem. 128 (1939) 537–550.

[21] M. Yaqoob, B. Folgado Biot, A. Nabi, P.J. Worsfold, Determination of nitrate and nitrite in freshwaters using flow-injection with luminol chemiluminescence detection, Luminescence 27 (2012) 419–425, https://doi.org/10.1002/bio.1366.

[22] O. Adegoke, M.A. Pereira-Barros, S. Zolotovskaya, A. Abdolvand, N. Nic Daeid, Aptamer-based cocaine assay using a nanohybrid composed of ZnS/Ag_2Se quantum dots, graphene oxide and gold nanoparticles as a fluorescent probe, Microchim. Acta (2020) 187:104, https://doi.org/10.1007/s00604-019-4101-6.

[23] H. Cheng, S. Lin, F. Muhammad, Y.-W. Lin, H. Wei, Rationally modulate the oxidase-like activity of nanoceria for self-regulated bioassays, ACS Sens. 1 (2016) 1336-1343, https://doi.org/10.1021/acssensors.6b00500.

[24] A. Lerf, H. He, M. Forster, J. Klinowski, Structure of graphite oxide revisited, J. Phys. Chem. B 102 (1998) 4477–4482, https://doi.org/10.1021/jp9731821.

[25] B. Liu, S. Salgado, V. Maheshwari, J. Liu, Janus DNA orthogonal adsorption of graphene oxide and metal oxide nanoparticles enabling stable sensing in serum, Curr. Opin. Colloid Interface 26 (2016) 41–49, https://doi.org/10.1039/C7MH00804J.

[26] Z. Çiplak, N. Yildiz, A. Çalimli, Investigation of graphene/Ag nanocomposites synthesis parameters for two different synthesis methods, Fullerenes, Nanotub. Carbon Nanostruct. 23 (2014) 361–370, https://doi.org/10.1080/1536383X.2014.894025.

[27] H. Bisswanger, Enzyme assays, Perspect. Sci 1 (2014) 41–55, https://doi.org/10.1016/j.pisc.2014.02.005.

[28] A. Dalui, B. Pradhan, U. Thupakula, A.H. Khan, G.S. Kumar, T. Ghosh, B. Satpati, S. Acharya, Insight into the mechanism revealing the peroxidase mimetic catalytic activity of quaternary CuZnFeS nanocrystals: colorimetric biosensing of hydrogen peroxide and glucose, Nanoscale 7 (2015) 9062-9074, https://doi.org/10.1039/C5NR01728A.

[29] H. Liu, Y. Ding, B. Yang, Z. Liu, Q. Liu, X. Zhang, Colorimetric and ultrasensitive detection of H_2O_2 based on Au/Co_3O_4-CeO_x nanocomposites with enhanced peroxidase-like performance, Sens. Actuators B Chem. 271 (2018) 336-345, https://doi.org/10.1016/j.snb.2018.05.108.

[30] M. Finnegan, E. Linley, S.P. Denyer, G. McDonnell, C. Simons, J.-Y. Maillard, Mode of action of hydrogen peroxide and other oxidizing agents: differences between liquid and gas forms. J. Antimicrob. Chemother. 65 (2010) 2108-2115, https://doi.org/10.1093/jac/dkq308.

[31] K.I. Ishibashi, A. Fujishima, T. Watanabe, K. Hashimoto, Detection of active oxidative species in TiO_2 photocatalysis using the fluorescence technique, Electrochem. Commun. 2 (2000) 207−210, https://doi.org/10.1016/S1388-2481(00)00006-0.

[32] T.T. Ngo, Peroxidase in chemical and biochemical analysis, Anal. Lett. 43 (2010) 1572-1587, https://doi.org/10.1080/00032711003653874.

[33] A.M. Asira, W.A. Adeosun, M.M. Rahman, Development of highly efficient non-enzymatic nitrite sensor using La_2CuO_4 nanoparticles, Microchim. J. 159 (2020) 105527, https://doi.org/10.1016/j.microc.2020.105527.

[34] Md. S. Alam, M.M. Rahman, H.M. Marwani, M.A. Hasnat, Insights of temperature dependent catalysis and kinetics of electro-oxidation of nitrite ions on a glassy carbon electrode, Electrochim. Acta 362 (2020) 137102, https://doi.org/10.1016/j.electacta.2020.137102.

[35] Md. R. Awual, Md. M. Hasan, A. Islam, M.M. Rahman, A.M. Asiri, Md. A. Khaleque, Md. C. Sheikh, Introducing an amine functionalized novel conjugate material for toxic nitrite detection and adsorption from wastewater, J. Clean. Prod. 228 (2019) 778-785, https://doi.org/10.1016/j.jclepro.2019.04.280.

[36] Md. R. Awual, A.M. Asiri, M.M. Rahman, N.H. ALharthi, Assessment of enhanced nitrite removal and monitoring using ligandmodified stable conjugate materials, Chem. Eng. J. 363 (2019) 64-72, https://doi.org/10.1016/j.cej.2019.01.125.

[37] Md. S. Alam, Md. F. Shabik, M.M. Rahman, M. del Valle, M.A. Hasnat, Enhanced electrocatalytic effects of Pd particles immobilized on GC surface on the nitrite oxidation reactions, J. Electroanal. Chem. 839 (2019) 1-8, https://doi.org/10.1016/j.jelechem.2019.02.058.

[38] A.M. Asiri, W.A. Adeosun, H.M. Marwani, M.M. Rahman, Homopolymerization of 3-aminobenzoic acid for enzyme-free electrocatalytic assay of nitrite ions, New J. Chem, 44 (2020) 2022-2032, https://doi.org/10.1039/C9NJ06058H.

[39] WHO guidelines for drinking-water quality, Nitrate and nitrite in drinking-water, WHO/FWC/WSH/16.52, 2016.

[40] T. Tomiyasu, Y. Konagayoshi, K. Anazawa, H. Sakamoto, A kinetic method for the determination of nitrite by its catalytic effect on the oxidation of chlorpromazine with nitric acid, Anal. Sci. 17 (2001) 1437-1440, https://doi.org/10.2116/analsci.17.1437.

[41] H.Z. Mousavi, H. Shirkhanloo, Spectrophotometric determination of nitrite based on its catalytic effect on the reaction of nuclear fast red and potassium nitrate, J. Serb. Chem. Soc. 74 (2009) 985-992, https://doi.org/10.2298/JSC0909985M.

[42] W. L. Daniel, M. S. Han, J. S. Lee and C. A. Mirkin, Colorimetric nitrite and nitrate detection with gold nanoparticle probes and kinetic end points, J. Am. Chem. Soc., 2009, 131, 6362-6363, https://doi.org/10.1021/ja901609k.

[43] N. Xiao, C.X. Yu, Rapid-response and highly sensitive noncross-linking colorimetric nitrite sensor using 4-aminothiophenol modified gold nanorods. Anal. Chem. 82 (2010) 3659-3663, https://doi.org/10.1021/ac902924p.

[44] T.M.G. Cardoso, P.T. Garcia, W.K.T. Coltro, Colorimetric determination of nitrite in clinical, food and environmental samples using microfluidic devices stamped in paper platform, Anal. Methods 7 (2015) 7311-7317, https://doi.org/10.1039/C5AY00466G.

Table 1. Comparison of the analytical performance of the AuNP-CeO_2 NP@GO catalytic colorimetric sensor with published analytical parameters for nitrite detection.

Method	Probe	LOD (µg/mL)	Assay time	Ref.
Catalytic spectrometry	Chlorpromazine	1.2	-	**40**
Catalytic spectrometry	Nuclear fast red	0.7	5 min	**41**
Colorimetry	AuNPs	1.4	25 min	**42**
Colorimetry	Au nanorods	0.7	10 min	**43**
Colorimetry with microfluidics	Modified Griess reaction	~0.4	15 min	**44**
Catalytic nanozyme colorimetry	AuNP-CeO_2 NP@GO	0.3	1 min 30 sec	**This work**

Table 2. Analytical performance of the AuNP-CeO_2 NP@GO catalytic colorimetric sensor towards nitrite detection in tap water.

Spiked nitrite (µM)	Found (µM)	Recovery (%) ±SD (%)	RSD (%)
5000	3833	77±2	1.7
3000	2028	68±3	0.3
1000	761	76±4	0.7
500	437	88±2	0.4

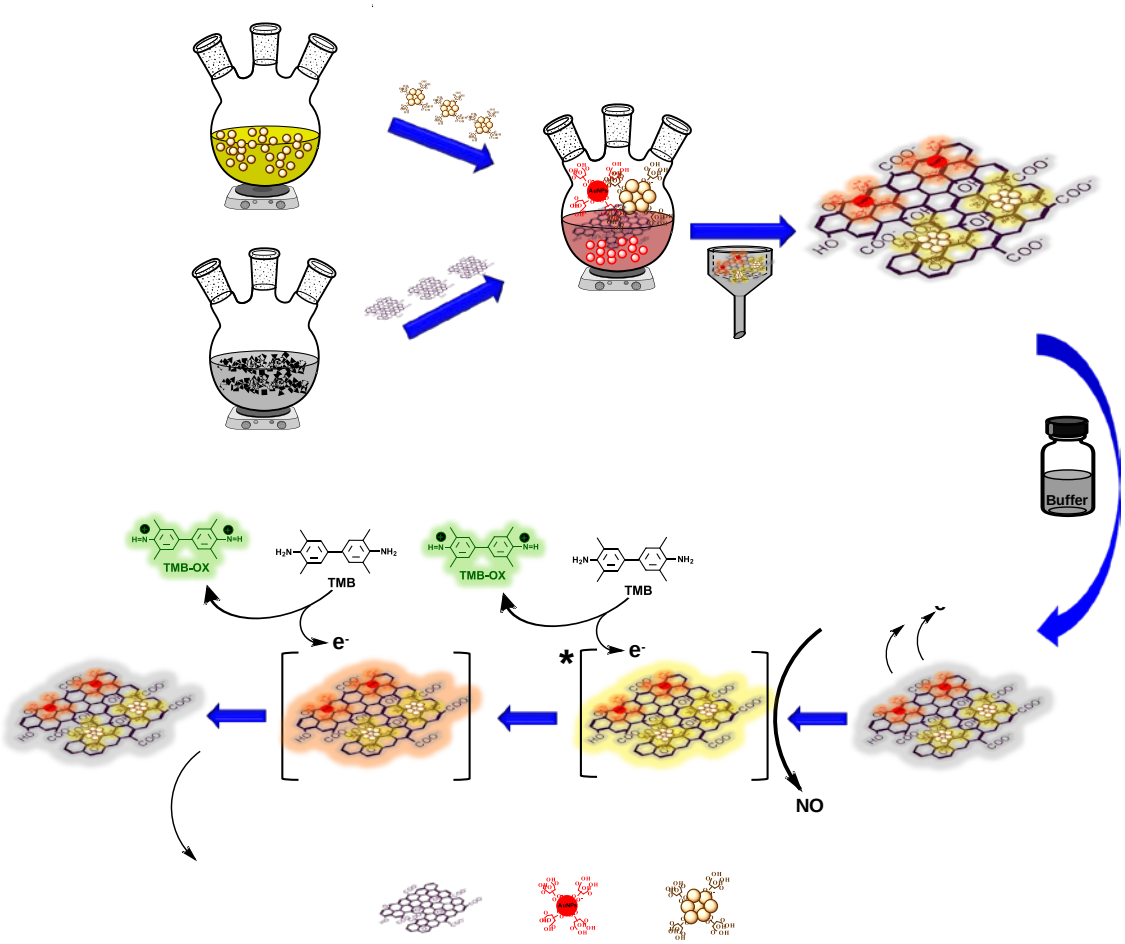

Scheme 1. Schematic description of the AuNP-CeO_2 NP@GO nanohybrid preparation and its use as an artificial enzyme mimic for the catalytic colorimetric detection of nitrite. Citrate-CeO_2 NPs were synthesized via the hydrothermal method while GO was synthesized via the chemical oxidation of graphite to graphite oxide and the subsequent chemical exfoliation of graphite oxide. During the chemical reduction of Au salt to form AuNPs, solutions of GO and CeO_2 NPs were incorporated into the growth solution to aid adsorption of AuNPs and CeO_2 NPs onto GO nanosheets. Nitrite driven initiation of the AuNP-CeO_2 NP@GO redox cycle occurs via the creation of a high oxidative [AuNP-CeO_2 NP@GO]* which serve as the main driving oxidative force in converting colourless TMB to a green oxidative product. Through the redox cycle route, [AuNP-CeO_2 NP@GO]* is reduced via a TMB molecule leading to the formation of lower oxidative intermediate in the form of [AuNP-CeO_2 NP@GO]**. [AuNP-CeO_2 NP@GO]** is subsequently reduced via another TMB molecule and returned to the original AuNP-CeO_2 NP@GO form.

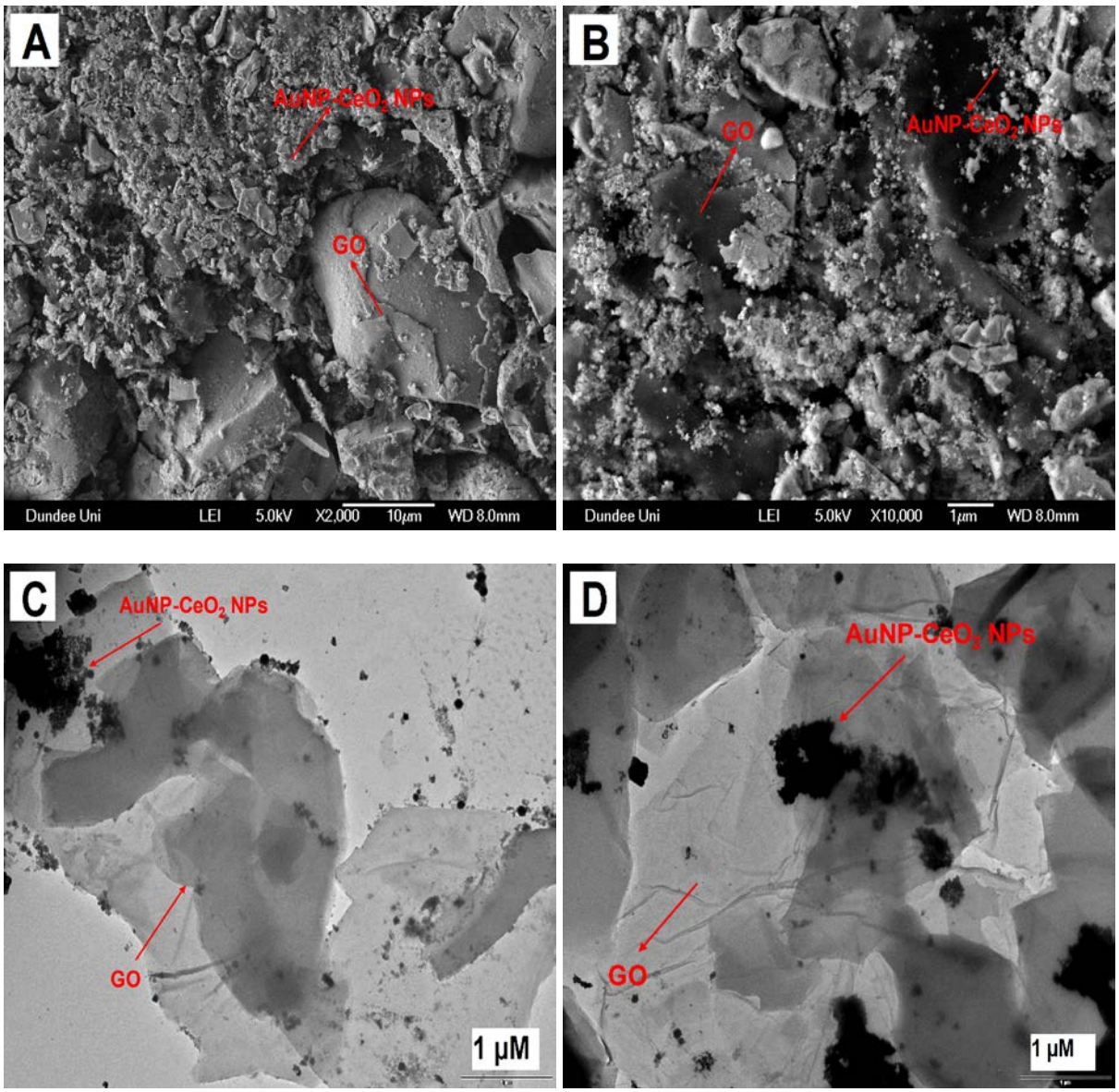

Fig. 1. SEM images at different magnifications (A and B) and TEM images taken at different grid positions (C and D) of the synthesized AuNP-CeO_2 NP@GO nanohybrid material.

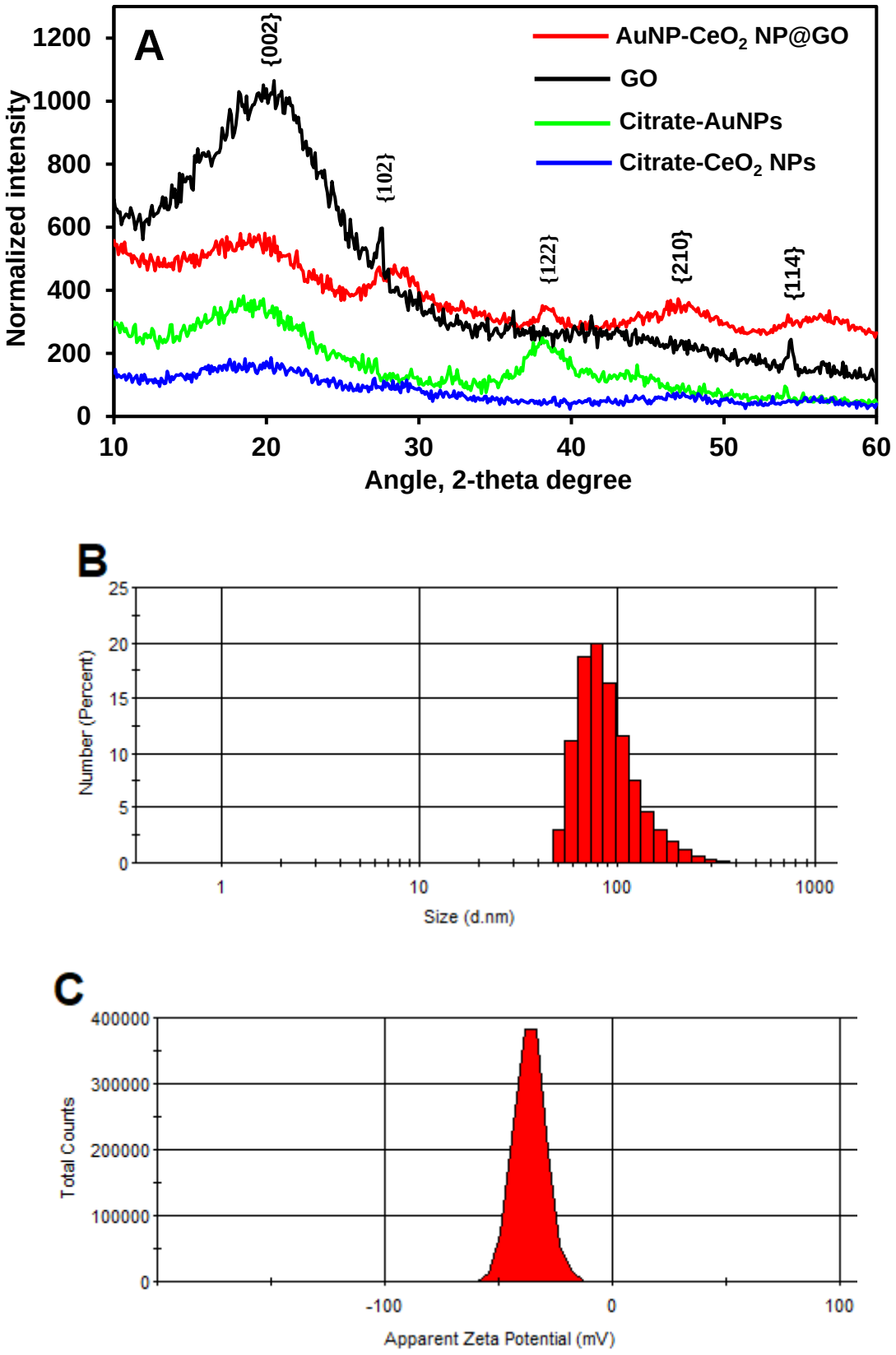

Fig. 2. XRD pattern of CeO_2 NP, GO, cit-AuNPs and AuNP-CeO_2 NP@GO nanohybrid. (B) DLS histogram and (B) zeta potential plots of AuNP-CeO_2 NP@GO nanohybrid.

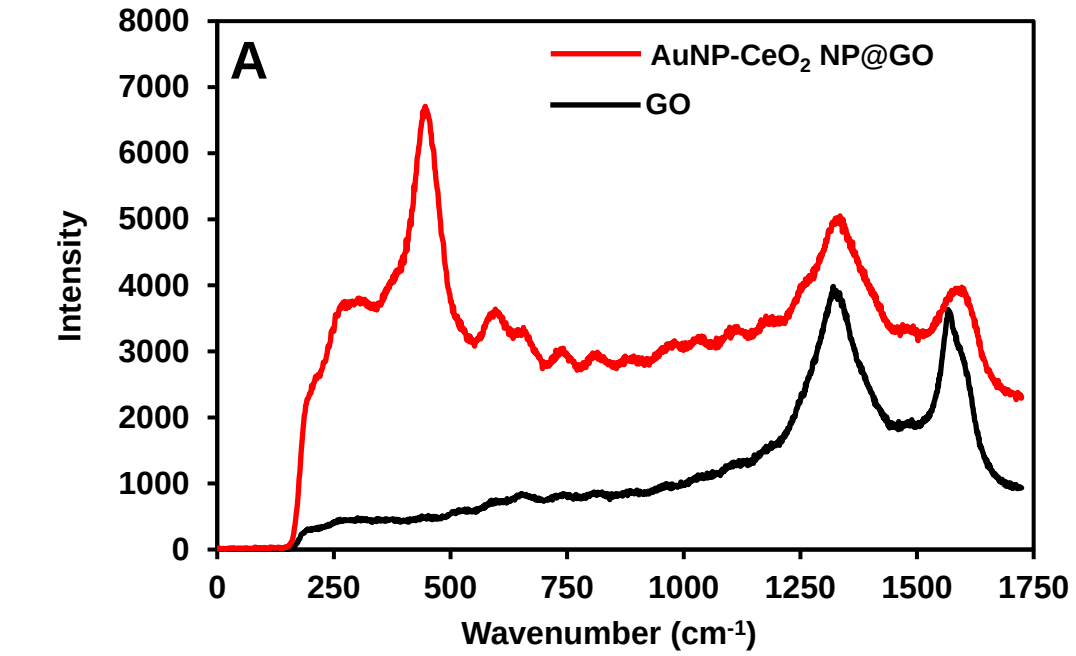
A
AuNP-CeO2 NP@GO
GO
Intensity
Wavenumber (cm-1)
8000
7000
6000
5000
4000
3000
2000
1000
0
0
250
500
750
1000
1250
1500
1750

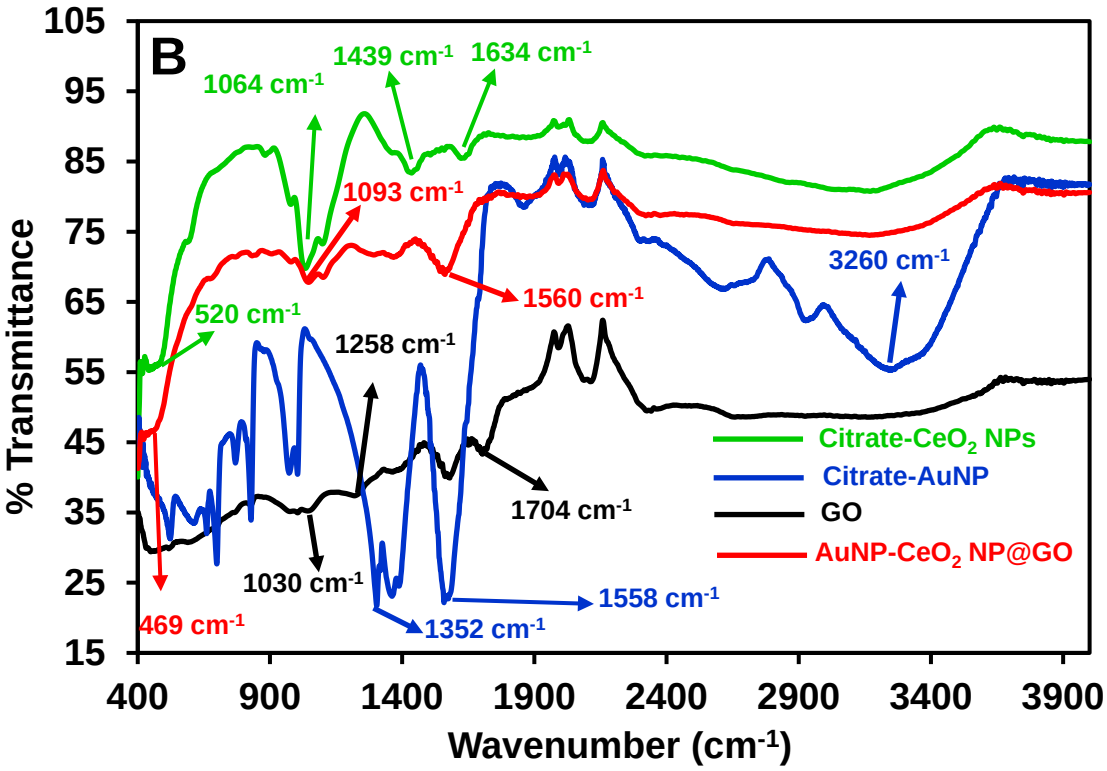
B
1064 cm-1
1439 cm-1
1634 cm-1
1093 cm-1
1560 cm-1
3260 cm-1
520 cm-1
1258 cm-1
1704 cm-1
1030 cm-1
469 cm-1
1352 cm-1
1558 cm-1
Citrate-CeO2 NPs
Citrate-AuNP
GO
AuNP-CeO2 NP@GO
% Transmittance
Wavenumber (cm-1)
105
95
85
75
65
55
45
35
25
15
400
900
1400
1900
2400
2900
3400
3900

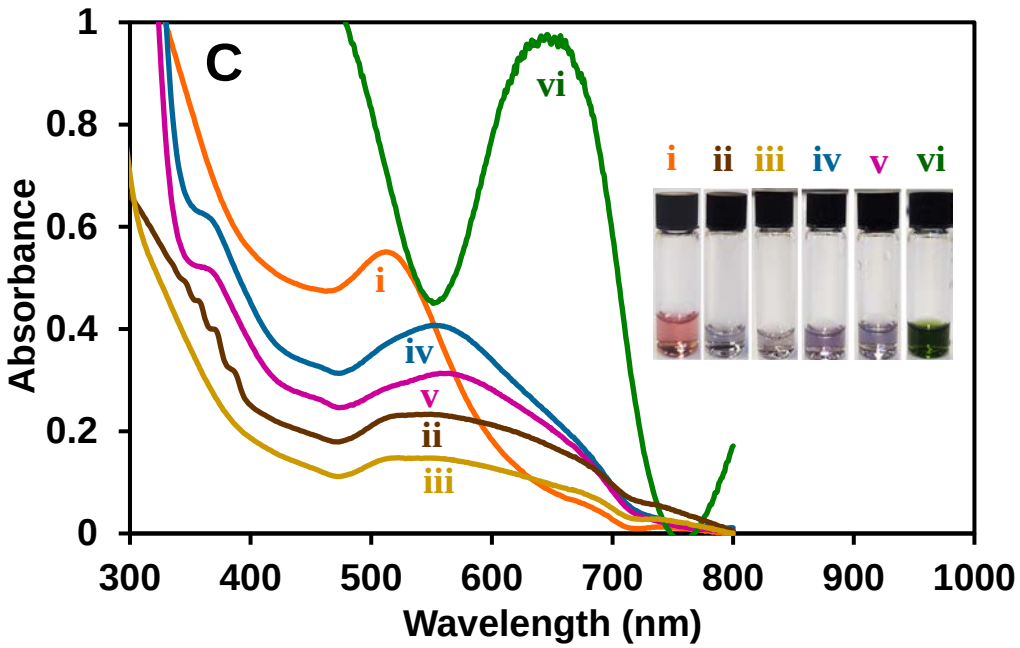

Fig. 3. (A) Raman spectra of GO and AuNP-CeO_2 NP@GO nanohybrid. (B) FTIR spectra of citrate-CeO_2 NPs, citrate-AuNPs, GO and AuNP-CeO_2 NP@GO nanohybrid. (C) U`V/vis absorption spectra of AuNP-CeO_2 NP@GO nanozyme (i), AuNP-CeO_2 NP@GO + nitrite (ii), AuNP-CeO_2 NP@GO + buffer (iii), AuNP-CeO_2 NP@GO + TMB (1.2 mM) (iv), AuNP-CeO_2 NP@GO + TMB + MES-BIS-TRIS Trisma Ac-citric acid, pH 2.0 buffer (no nitrite) (v) and AuNP-CeO_2 NP@GO + TMB (1.2 mM) + nitrite (5000 µM) in MES-BIS-TRIS Trisma Ac-citric acid, pH 2.0 buffer (vi). [AuNP-CeO_2 NP@GO] = 0.02 nM.

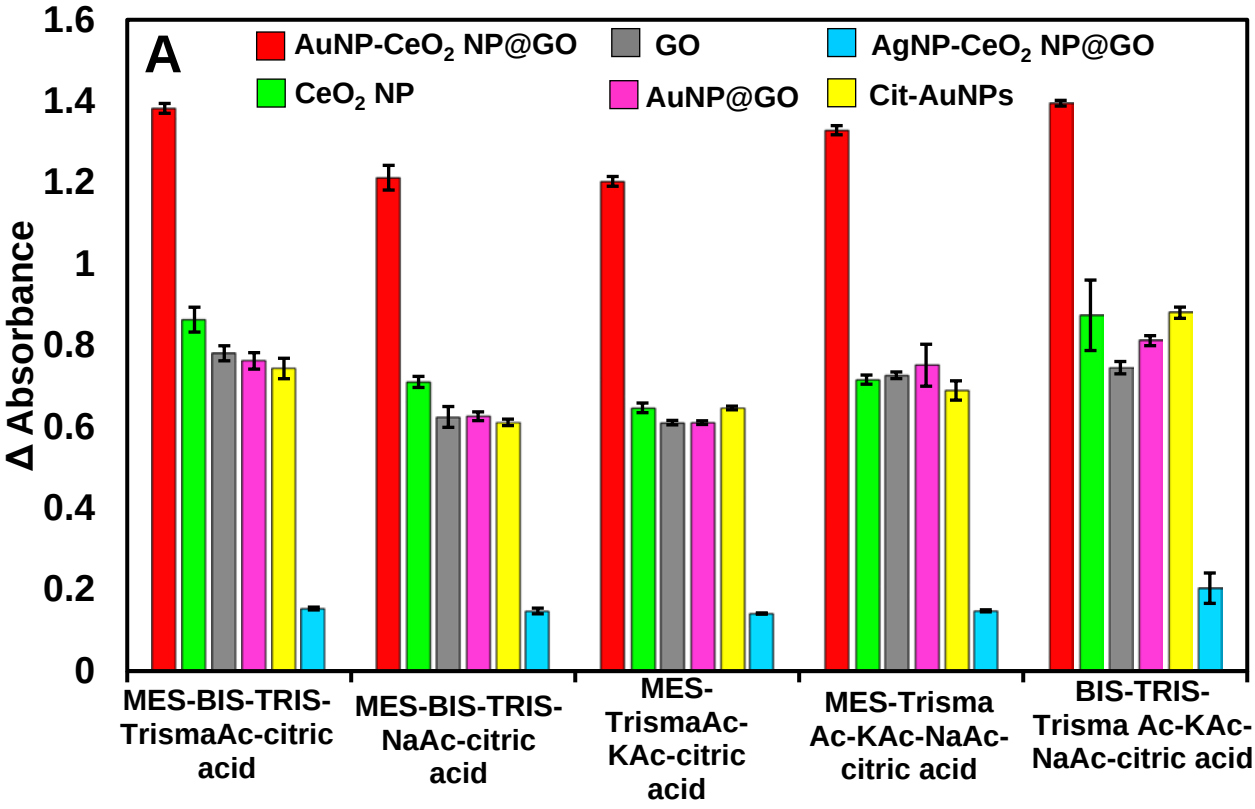
A
AuNP-CeO2 NP@GO
GO
AgNP-CeO2 NP@GO
CeO2 NP
AuNP@GO
Cit-AuNPs
Δ Absorbance
1.6
1.4
1.2
1
0.8
0.6
0.4
0.2
0
MES-BIS-TRIS-TrismaAc-citric acid
MES-BIS-TRIS-NaAc-citric acid
MES-TrismaAc-KAc-citric acid
MES-Trisma Ac-KAc-NaAc-citric acid
BIS-TRIS-Trisma Ac-KAc-NaAc-citric acid

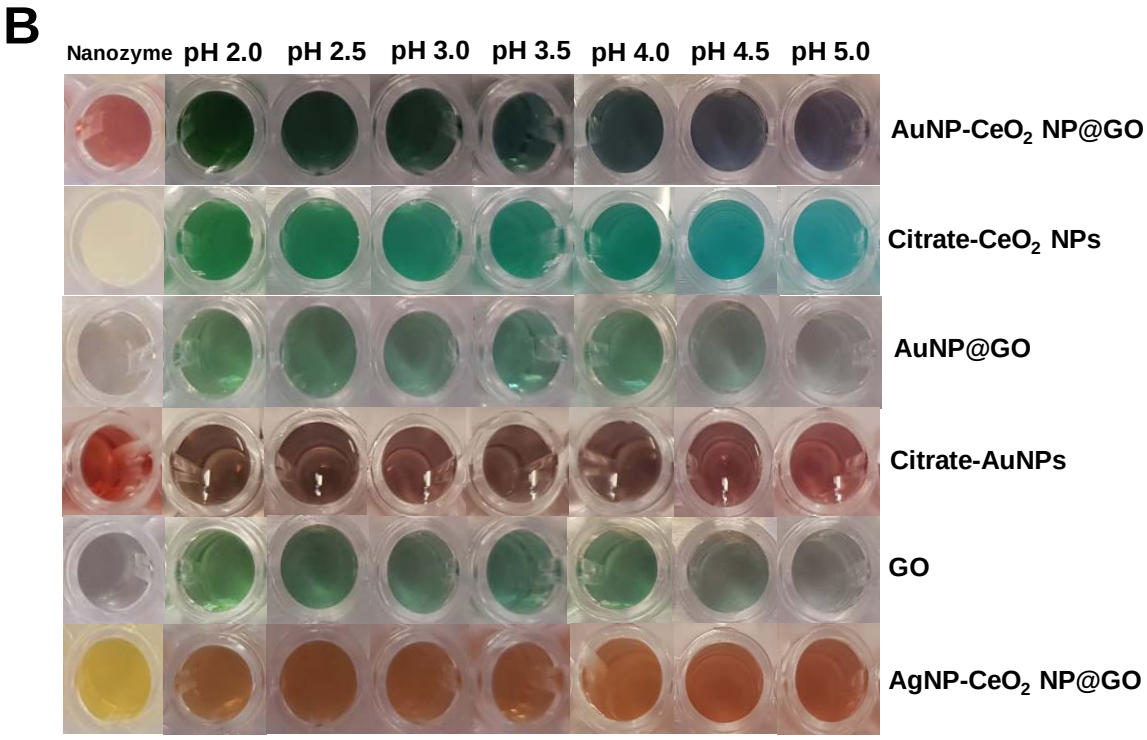
B
Nanozyme
pH 2.0
pH 2.5
pH 3.0
pH 3.5
pH 4.0
pH 4.5
pH 5.0
AuNP-CeO2 NP@GO
Citrate-CeO2 NPs
AuNP@GO
Citrate-AuNPs
GO
AgNP-CeO2 NP@GO

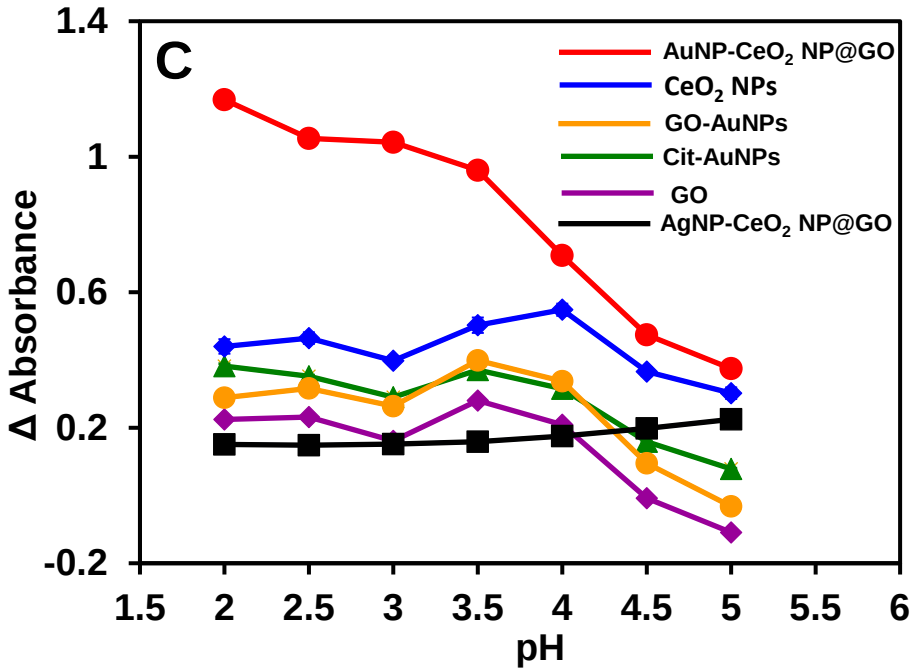

Fig. 4. (A) Comparative colorimetric catalytic absorbance signal of the AuNP-CeO_2 NP@GO hybrid nanozyme with other nanomaterials for nitrite detection in different buffer systems. Comparative photographic colorimetric response (B) and the corresponding absorbance plots (C) of the AuNP-CeO_2 NP@GO hybrid nanozyme with other nanomaterials for nitrite detection at different pH; Δ Absorbance = Absorbance $_{\text{nitrite catalytic signal}}$ – Absorbance $_{\text{nanozyme}}$. [Nitrite] = 5000 µm. Note: Catalytic absorbance signal for Fig. 4A and C was read from the 800 TS microplate absorbance reader at a filter wavelength of 650 nm.

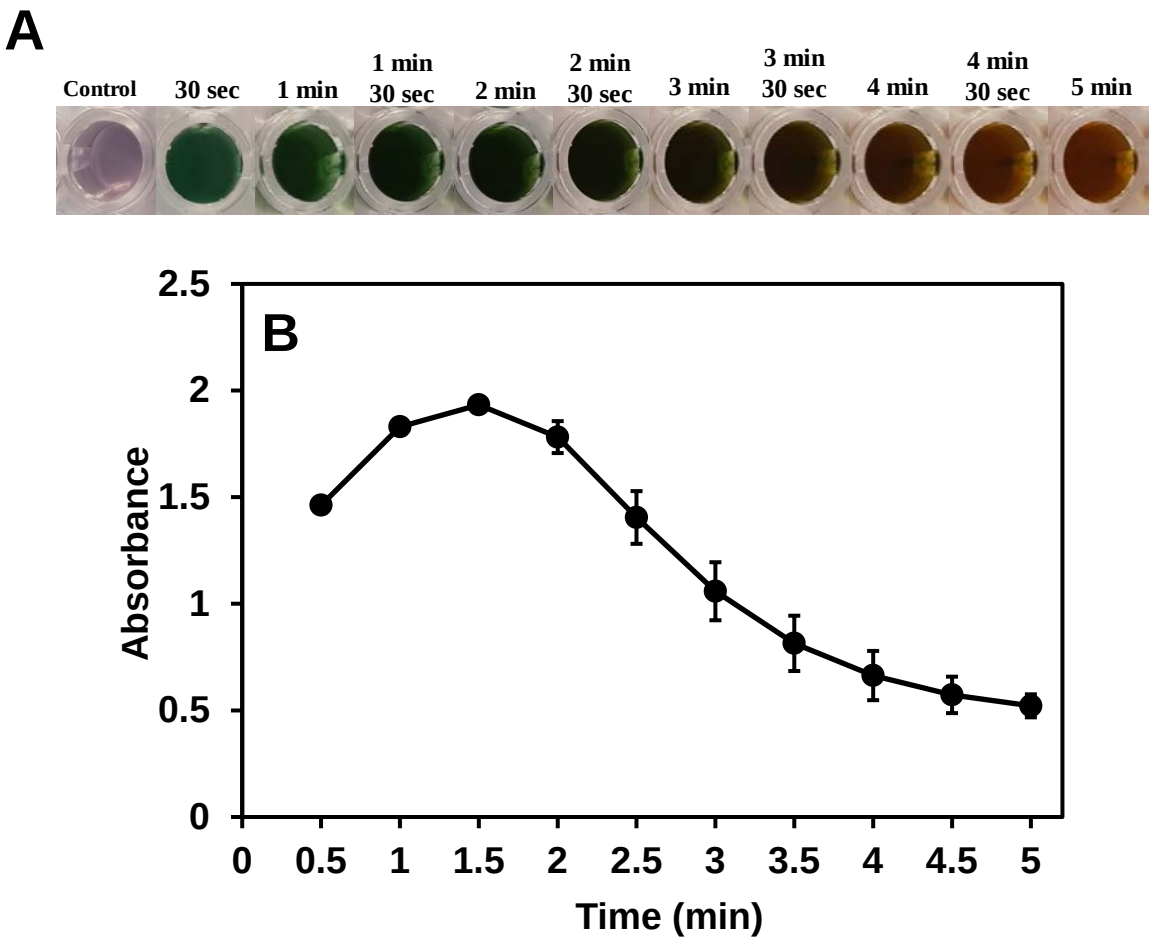

Fig. 5. (A) Photographic colorimetric response of the AuNP-CeO_2 NP@GO nanozyme to nitrite detection at different incubation time and the (B) corresponding catalytic absorbance signal generated at the different detection time. Control = AuNP-CeO_2 NP@GO nanozyme + TMB (1.2 mM) + MES-BIS-TRIS Trisma Ac-citric acid, pH 2.0 buffer. [Nitrite] = 5000 µm. [AuNP-CeO_2 NP@GO nanozyme] = Nitrite] = 5000 µM. Note: Catalytic absorbance signal for Fig. 5C was read from the 800 TS microplate absorbance reader at a filter wavelength of 650 nm.

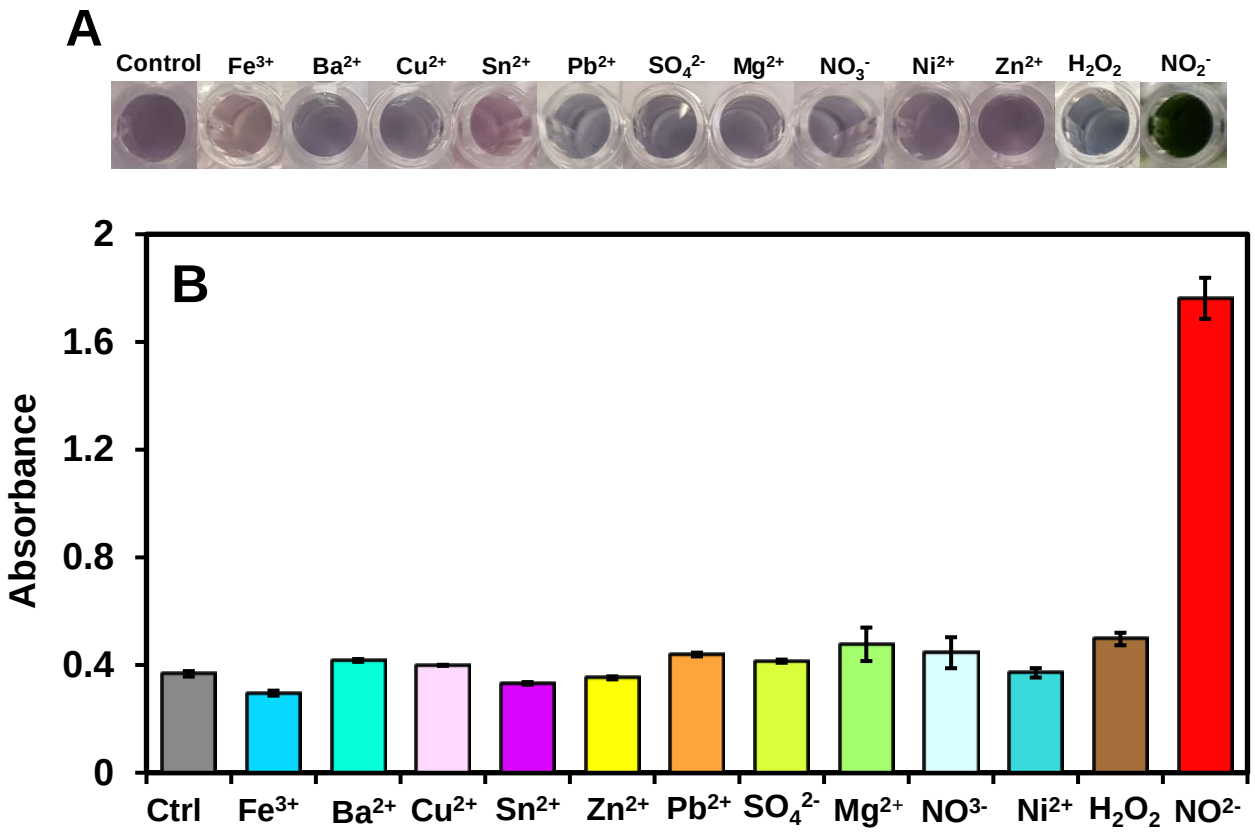

Fig. 6. (A) Photographic colorimetric response of the AuNP-CeO_2 NP@GO nanozyme to nitrite detection in comparison to other analytes and (B) the corresponding absorbance signal generated from the colorimetric reaction for nitrite compared to other analytes. Control = AuNP-CeO_2 NP@GO nanozyme + TMB (1.2 mM) + MES-BIS-TRIS Trisma Ac-citric acid, pH 2.0 buffer. [Nitrite and other analytes] = 5000 µM. Note: Catalytic absorbance signal for Fig. 6B was read from the 800 TS microplate absorbance reader at a filter wavelength of 650 nm.

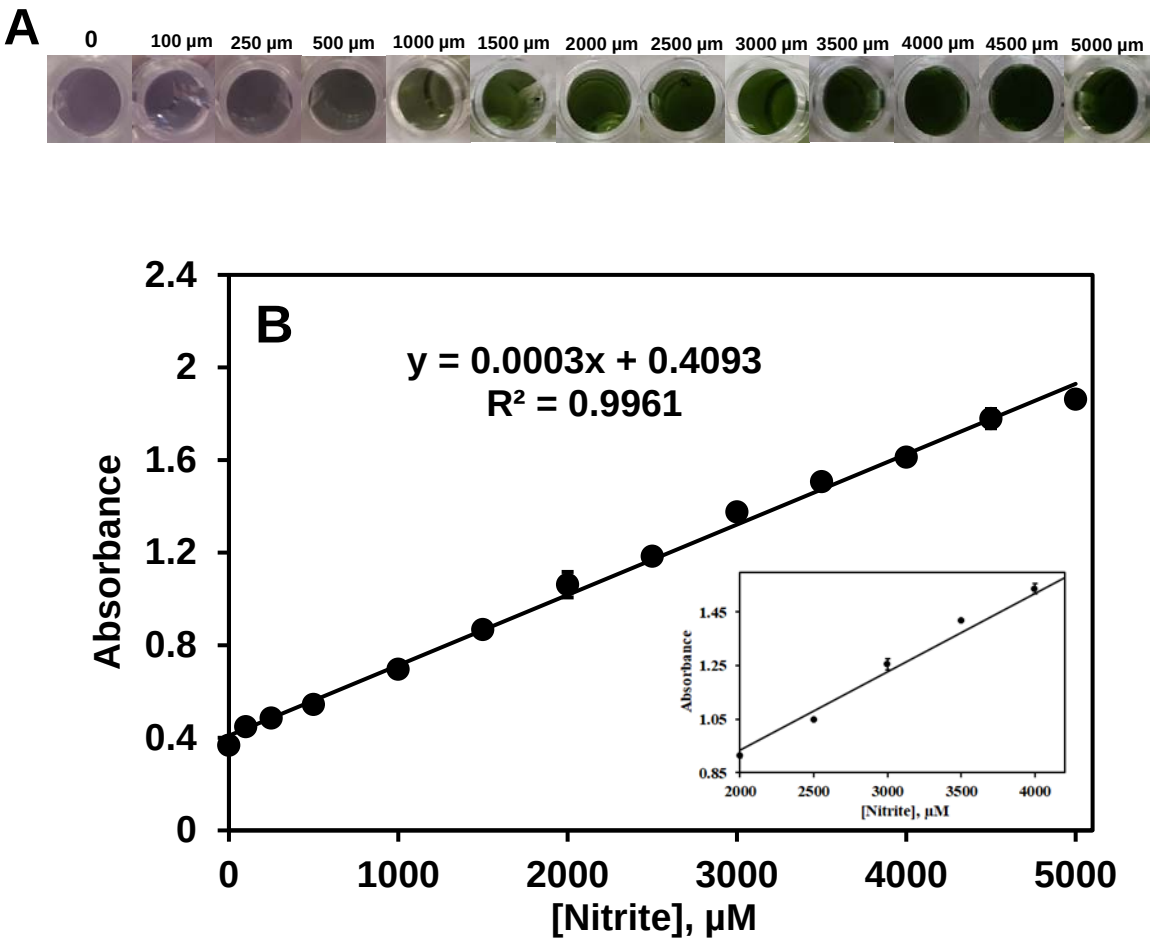

Fig. 7. Photographic colorimetric response of the AuNP-CeO_2 NP@GO nanozyme to nitrite quantitative detection and (B) the corresponding absorbance signal generated from the colorimetric nitrite quantitative detection. Control = AuNP-CeO_2 NP@GO nanozyme + TMB (1.2 mM) + MES-BIS-TRIS Trisma Ac-citric acid, pH 2.0 buffer. Note: Catalytic absorbance signal for Fig. 7B was read from the 800 TS microplate absorbance reader at a filter wavelength of 650 nm. Inset: Projected view of a section of the linear regression plot to show the error bars.